

Cite this: *Biomater. Sci.*, 2018, 6, 827

Co-administration of genistein with doxorubicin-loaded polypeptide nanoparticles weakens the metastasis of malignant prostate cancer by amplifying oxidative damage†

Guanyi Wang,^{a,b} Dawei Zhang,^b Shengcai Yang,^b Yalin Wang,^b Zhaohui Tang ^{*b} and Xueqi Fu ^{*a}

Prostate cancer is a typical malignant disease with a high incidence and a poor prognosis. Doxorubicin hydrochloride (DOX-HCl) is one of the most effective agents in the treatment of prostate cancer, but severe side effects and metastasis after its treatment impose restrictions on its application. Herein, a combination of genistein (GEN) and doxorubicin-loaded polypeptide nanoparticles (DOX-NPs) is constructed for the treatment of prostate cancer. The DOX-NPs can reduce the side effects caused by free DOX-HCl and produce a relatively low level of intracellular reactive oxygen species (ROS)-induced oxidative damage, while GEN, an inhibitor of the oxidative DNA repair enzyme apurinic/aprimidinic endonuclease1 (APE1), can further amplify the ROS-induced oxidative damage by downregulating the intracellular expression of APE1 and reducing oxidative DNA repair in the prostate cancer cells. Because high levels of ROS-induced oxidative damage can prevent the distant metastasis of tumor cells, the distant metastasis of malignant prostate cancer cells is significantly inhibited by the combination of genistein and DOX-NPs with amplified oxidative damage.

Received 22nd December 2017,
Accepted 8th February 2018

DOI: 10.1039/c7bm01201b

rscl.li/biomaterials-science

Introduction

Prostate cancer is a typical malignant disease that affects men. In 2012, worldwide, there were 1.1 million men diagnosed with prostate cancer, accounting for 15% of all incident cancer cases in men.^{1,2} The treatment of prostate cancer is still challenging; it is the fifth leading cause of death from cancer in men. Most prostate cancer patients die of tumor metastasis because malignant prostate carcinoma cells are able to metastasize from a primary focus to a metastatic focus, located at the rectum, bladder, bones, lymph nodes, lungs, or liver.^{3,4} Therefore, a new paradigm for treating prostate cancer is badly in need of being sought out.

Doxorubicin hydrochloride (DOX-HCl), a conventional chemotherapy drug, is considered to be one of the most effective agents for the treatment of prostate cancer.⁴ However,

the application of DOX-HCl can lead to severe side effects, such as cardiotoxicity and nephrotoxicity. Furthermore, metastasis is often observed after DOX-HCl treatment. The shortcomings of DOX-HCl must be compensated in prostate cancer therapy. The side effects caused by DOX-HCl can be reduced significantly by using nanocarrier-based drug delivery systems.⁴⁻⁷ In addition, it has been reported that oxidative damage has the potential to inhibit the distant metastasis of tumor cells.^{8,9} An elevated level of reactive oxygen species (ROS) can cause oxidative DNA damage.¹⁰⁻¹² It is well known that tumor cells treated by DOX-HCl will produce elevated levels of ROS and oxidative DNA damage. However, many kinds of prostate cancer cells have an elevated DNA repair capacity, resulting in tumor malignancy and imposing severe restrictions on the anticancer efficacy of DOX-HCl, which is a fundamental reason for the failure for prostate cancer treatment.¹³ Apurinic/aprimidinic endonuclease 1 (APE1), a pivotal enzyme in the base excision repair (BER) pathway, is overexpressed in tumor tissue and responsible for the DNA repair of oxidative DNA damage.¹⁴⁻¹⁷ The downregulation of APE1 can improve the level of reactive oxygen species,^{18,19} and enhance drug sensitivity and oxidative damage towards tumor cells.^{18,20-25} Thus, APE1 is a promising target for cancer therapy.^{26,27} Therefore, while reducing the cardiotoxicity and nephrotoxicity of DOX-HCl through nanotechnology, it is of

^aEdmond H. Fischer Signal Transduction Laboratory, College of Life Sciences, Jilin University, 2699 Qianjin Street, Changchun, 130012, P. R. China.

E-mail: fxq@jlu.edu.cn; Fax: +86-431-85155321; Tel: +86-431-85155321

^bKey Laboratory of Polymer Ecomaterials, Changchun Institute of Applied Chemistry, Chinese Academy of Sciences, 5625 Renmin Street, Changchun, 130022, P. R. China.

E-mail: ztang@ciac.ac.cn; Fax: +86-431-85262116; Tel: +86-431-85262116

†Electronic supplementary information (ESI) available. See DOI: 10.1039/c7bm01201b

importance to depress the function of APE1 in the treatment of prostate cancer.

Recently, epidemiological studies have suggested that Asian men could be more likely to avoid prostate cancer than American men, due to Asian men consuming diets rich in soybeans.² Genistein (GEN), a bioactive component in soy isoflavones, has shown versatile pharmacological and medical efficacy towards multiple cancer cells.^{28–31} A large amount of literature has argued for the standpoint that GEN is an inhibitor of APE1.^{28,32}

Polymeric nanocarrier-based drug delivery systems are important in the treatment of metastatic cancers.^{33–36} In this work, an experimental mouse model was established by subcutaneously transplanting the mouse prostate cancer cell line RM-1 in order to mimic malignant prostate tumors along with rapid proliferation and metastasis.^{4,37} A combination of free GEN and DOX-NPs was designed for the treatment of the metastatic prostate cancer. An amphiphilic anionic copolymer, methoxy poly (ethylene glycol)-*b*-poly (L-glutamic acid-*co*-L-phenylalanine) (mPEG-*b*-P(Glu-*co*-Phe)) was used to load free DOX-HCl. On one hand, the prepared DOX-NPs could reduce the side effects of free DOX-HCl. On the other hand, the DOX-NPs could enhance intracellular ROS levels and produce oxidative damage. Meanwhile, the utilization of GEN, as an adjuvant drug of the DOX-NPs, could downregulate the intracellular expression of APE1, enhance ROS levels in the prostate cancer cells, and reduce the DNA damage repair, further amplifying oxidative damage and inhibiting the distant metastasis of prostate cancer cells (Fig. 1).

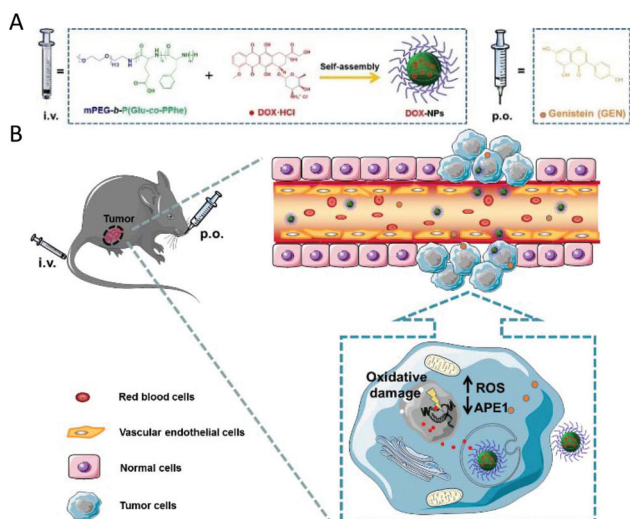


Fig. 1 A schematic representation of the co-administration of GEN and DOX-NPs for prostate cancer treatment. (A) GEN and DOX-NPs were administrated *via* oral administration (p.o.) and intravenous injection in the tail (i.v.), respectively. (B) GEN and DOX-NPs were internalized by the prostate cancer cells, resulting in the decrease of APE1 and the increase of intracellular ROS. The combined treatment amplified oxidative damage.

Experimental section

Materials

Doxorubicin hydrochloride (DOX-HCl) was bought from Beijing Huafeng United Technology Co., Ltd (Beijing, P. R. China). Genistein (GEN) was bought from TCI (Shanghai) Development Co., Ltd (Shanghai, P. R. China). 3-(4,5-Dimethylthiazol-2-yl)-2,5-diphenyl tetrazolium bromide (MTT) and 4',6-diamidino-2-phenylindole dihydrochloride (DAPI) were purchased from Sigma-Aldrich (Shanghai, P. R. China). All of the RT-PCR experimental kits were purchased from Tian-gen Biotech Co., Ltd (Beijing, P. R. China).

The mPEG-*b*-P(Glu-*co*-Phe) copolymer was prepared as reported previously,³⁸ with 113 EG (ethylene glycol), 10 Phe, and 10 Glu units in the polypeptide block. ¹H NMR measurements indicated that the number average molecule weight (M_n) of mPEG-*b*-P(Glu-*co*-Phe) was 7.76×10^3 . GPC analysis revealed that the copolymer had a narrow molecular weight distribution (poly dispersity index (PDI, M_w/M_n) = 1.1).

The mouse prostate cancer cell line RM-1 was obtained from the Cell Bank of the Chinese Academy of Sciences (Shanghai, P. R. China). The RM-1 cells were cultured in a humid environment with a 5% CO₂ atmosphere at 37 °C, and the culture medium was DMEM medium (Gibco) to which 10% fetal bovine serum (FBS, Clake), 100 U mL⁻¹ penicillin, and 100 U mL⁻¹ streptomycin was added.

Preparation of DOX-NPs

The nanoformulation of DOX-HCl was prepared by a method similar to that which we reported before, but with slight modification.³⁸ Briefly, mPEG-*b*-P(Glu-*co*-Phe) (720.0 mg) was dissolved in 13 mL distilled water and the pH was adjusted to 7.0–7.5 by adding 0.1 M NaOH solution. Then, DOX-HCl (80.0 mg) in 17 mL distilled water was added to the solution drop-wise under mild stirring. After 2 h, the solution was transferred to a dialysis bag (MWCO 3500 Da), and dialyzed for 24 h to remove free DOX-HCl. The solution in the dialysis bag was centrifuged at 9000 rpm for 7 min. Then, the supernatant was collected and filtered through a syringe filter (membrane filter 0.45 μm). After freeze-drying, DOX-NPs were obtained. The drug loading content (DLC %) and drug loading efficiency (DLE %) were determined by a UV-Vis spectrometer at 480 nm and calculated by eqn (1) and (2), respectively.

$$\text{DLC}\% = \frac{\text{Amount of DOX}}{\text{Total amount of NPs}} \times 100\% \quad (1)$$

$$\text{DLE}\% = \frac{\text{DOX content in NPs}}{\text{Theoretical DOX content in NPs}} \times 100\% \quad (2)$$

MTT assays

RM-1 cells were uniformly seeded in 96-well plates and underwent 24-hour cell monolayer adherent growth. The density was 6000 cells per well. Then, the cells were treated with specific drugs (free DOX-HCl, DOX-NPs (equivalent DOX-HCl dose), or GEN) at pre-defined gradient concentrations for another 24 or

48 h. Afterwards, 20 μL MTT solution (5.0 mg mL^{-1}) was added to each well of the plates and maintained for an additional 4 h incubation at 37°C . Subsequently, 150 μL DMSO was added into every well, followed by the removal of the culture medium. The plates were laid into a Bio-Rad 680 microplate reader and measured with an established pattern (vibration for 5 min to dissolve the formazan dye and detection of the optical density (OD) at 490 nm). Data are exhibited as the mean \pm standard deviation ($n = 4$). The wells treated with different drugs (free DOX-HCl, DOX-NPs, or GEN) were regarded as experimental wells, while those treated with only culture media as control wells. The relative cell viability (%) was defined as the ratio of the absorbance of the experimental wells and the absorbance of the control wells $\times 100\%$.

Real-time quantitative polymerase chain reaction (RT-PCR)

The fluorescence signals of the dye SYBR Green I were used to quantify gene expression. According to the manufacturer's protocol, the total RNA from each sample was extracted using a RNAPrep Pure Cell Kit from the RM-1 cells treated with different groups of drugs, then quantified to the same level and reverse transcribed into cDNA. Then, following instructions, a 20 μL real-time PCR reaction system (consisting of the acquired cDNA) was performed and reacted on the PCR instrument (Stratagene Mx 3005P, USA) using the primer pairs: APE1 (F-5'-ATGAAGAAATTGACCTCCGTAACC-3', R-5'-GTGTAAGCGTAGCAGTGTG-3') and GAPDH (F-5'-AGTGGCAAAGTGGAGATT-3', R-5'-GTGGAGTCATACTGGAACA-3'). The conditions of the PCR amplification were set at 1 cycle (95°C for 15 min) and 40 cycles (95°C for 10 s, 60°C for 20 s, and 72°C for 32 s). GAPDH was used as an internal reference to certify an equal concentration of cDNA in each sample. The data were managed and analyzed with a $2^{-\Delta\Delta\text{CT}}$ method.

Cellular uptake assay and cellular ROS detection

The RM-1 cells were seeded into 6 well plates at a density of 5×10^5 cells per well and underwent 24-hour cell monolayer adherent growth. Then, each well was washed with aseptic phosphate buffered saline (PBS) and incubated with fresh medium containing 10 μM DOX-HCl or DOX-NPs for another 1 or 3 h in the incubator. Subsequently, the RM-1 cells were digested, collected, and immediately assessed for a DOX-corresponding fluorescence signal by flow cytometry (FCM).

The cell processing methods for cellular ROS detection were similar to the above steps. Each well was incubated with fresh medium containing pre-defined concentrations of GEN for 24 h. The RM-1 cells were collected and mixed with a 10 μM DCFH-DA probe at 37°C for 20 min. Then, the collected cells were washed three times with PBS to scour off the dissociative DCFH-DA probe. The corresponding fluorescence intensity was analyzed by FCM according to the manufacturer's protocol.³⁹

Apoptosis analysis

To detect the influence of GEN on the apoptosis of prostate cancer cells, RM-1 cells were seeded and adhered overnight in

the 6-well plates. Upon reaching 70–80% cell confluence, the RM-1 cells were exposed to specific-concentration (0, 30, 60, 90, or 120 μM) GEN for 48 h. Afterwards, according to instructions, the collected cells from each group were re-suspended in PBS and the fluorescent dyes Annexin V-FITC and PI were added into each sample, and then each sample was incubated at 37°C for 5–15 min in the dark. The fluorescence intensity of each sample was immediately detected using FCM.

Tumor therapy study

The whole animal experiments were approved by the Care and Use of Animals Center of Jilin University. This study was strictly carried out under the Guidelines for the Laboratory Protocol of Animal Care and Use Committee, Jilin University. Every effort was made to minimize animal pain. All participants were informed of the purposes of the study and the risks associated with the procedures and abided by the "Laboratory animals – guidelines of welfare and ethics" drafted by China. C57BL/6 male mice (5–6 weeks of age) were provided by the Laboratory Animal Center of Jilin University. The C57BL/6 mice were subcutaneously injected with 2.0×10^6 RM-1 cells (suspended in 0.1 mL of phosphate-buffered saline) into the armpit of the right anterior limb. When the tumor volume reached 80 mm^3 , the mice were randomly divided into six groups (control, GEN, DOX-HCl, DOX-NPs, GEN + DOX-HCl, and GEN + DOX-NPs) and numbered in their ears ($n = 8$). The mice were dosed with 0.2 mL of PBS alone as a control. DOX-HCl and DOX-NPs were administrated at an equivalent DOX-HCl dose of 5 mg kg^{-1} in 0.2 mL of PBS through intravenous injection into the tail at a pre-defined time point. GEN was dissolved in 0.1 M Na_2CO_3 and mixed with sesame seed oil at a 2:1 ratio (v/v) before treatment to avoid irritation of the esophagus by the Na_2CO_3 . GEN was taken *via* p.o. by gavage at 0.45 mg per mouse on an empty stomach every other day. Control, DOX-HCl, and DOX-NPs only-treated groups received a mixture of 0.1 M Na_2CO_3 and sesame seed oil.³² The mice were monitored and tumor volumes and body weights were recorded. During treatment, tumor volumes were calculated by eqn (3), where a and b represent the longest and shortest diameter of the tumors, respectively.

$$\text{Tumor volume}(\text{mm}^3) = \frac{a \times b^2}{2} \quad (3)$$

At the end of the animal experiments, the mice were sacrificed and their major organ tissues were collected and low-temperature frozen for stand-by application.

Tissue distribution assessments of DOX-HCl and DOX-NPs

The RM-1 tumor-bearing C57BL/6 mice were injected with DOX-HCl or DOX-NPs (5 mg kg^{-1} DOX-HCl equivalent) at a volume of 0.2 mL (per 20 g body weight) *via* the tail vein. After the injection, the mice were sacrificed after 2, 6, or 12 h. The tumors and other major organ tissue (heart, liver, spleen, lungs, and kidneys) were collected. After rinsing with PBS three times, the excised tissues were visualized using a Maestro In Vivo Imaging System (Cambridge Research &

Instrumentation, Inc., Woburn, MA, USA) at excitation and emission wavelengths of 523 and 560 nm, respectively.

Tumor tissue ROS detection

Fresh tumor tissues from each group were excised into 1–2 mm³ sections and incubated with digestive liquids (0.25% trypsin and 200 U mL⁻¹ collagenases IV) under gentle vibration at 37 °C for about 6 h. The collected digestive solutions were ground and filtered at 100 mesh into a single cell. The single cell suspensions were processed, followed by the above cellular ROS detection steps using a DCFH-DA probe. The green fluorescence intensity of every sample was immediately detected and analyzed by FCM to measure the ROS level.

Histopathological and immune-histochemical evaluations

The tumors and other major organs (heart, liver, spleen, lungs, and kidneys) in each group were immersed in 4% (w/v) PBS buffered paraformaldehyde and embedded in paraffin. The paraffin-embedded tissues were cut to a thickness of around 5 μm for hematoxylin and eosin (H&E) staining and immune-histochemical evaluations. Immuno-histochemical analyses were performed using antibodies against APE1 (CST) and 8-hydroxyguanosine (8-oxo-dG, Abcam), respectively. Thereafter, TUNEL staining (keygen bioTECH) was carried out according to the manufacturer's protocol. The H&E staining was observed *via* a microscope (Nikon Eclipse Ti, Optical Apparatus Co., Ardmore, PA, USA), and the immunofluorescence was analysed *via* confocal laser scanning microscopy (CLSM; Carl Zeiss LSM 780, Jena, Germany). The levels of the immunofluorescence intensity were evaluated by Image J software.

Data analysis

Data are presented as the mean ± standard deviation (SD).

The statistical significance of these data was analyzed using SPSS 14.0 (SPSS Inc., Chicago, IL, USA). A **p* value <0.05 was considered statistically significant, and a ***p* value of <0.01 was considered extremely statistically significant.

Results and discussion

Preparation and characterization of the nanoformulations

Through electrostatic interaction, free DOX·HCl was encapsulated into the interior of the mPEG-*b*-P(Glu-*co*-Phe) nanoparticles. Therein, poly (phenylalanine) was used to provide hydrophobic/aromatic groups to stabilize the nanoparticles in the self-assembly process, and poly (glutamic acid) was used to provide anions to encapsulate the cationic chemotherapeutic drug.^{40,41}

The DLC and DLE of the prepared DOX-NPs were 6.71% and 67.1%. The hydrodynamic radius of the DOX-NPs in aqueous solution was about 74.0 nm, which met the nano-scale demand for passive targeting and facilitated the selective tumor accumulation by EPR effects.^{42,43}

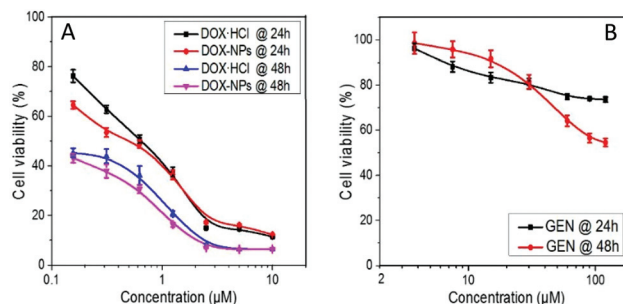


Fig. 2 The cytotoxicity of DOX-HCl and DOX-NPs (A), and GEN (B) against RM-1 cells at 24 h or 48 h (*n* = 4).

In vitro cytotoxicity against RM-1 prostate cells

As shown in Fig. 2, the MTT assay was used to estimate the cytotoxicity of the drugs against the RM-1 cells after treatment with free DOX·HCl, DOX-NPs, or GEN. Not only the cell cytotoxic drug doxorubicin hydrochloride and its nanoparticles (DOX-NPs), but also the bioactive component genistein from soy isoflavones had time- and dose-dependent cell cytotoxicity against the RM-1 cells. The IC₅₀ (inhibitory concentration to produce 50% cell death) of DOX·HCl and the DOX-NPs at 24 h was 0.647 μM and 0.451 μM, respectively. The IC₇₀ of DOX·HCl and the DOX-NPs at 48 h was 0.756 μM and 0.559 μM, respectively, which indicated that the DOX-NPs had a higher cytotoxicity against the RM-1 cells than free DOX·HCl. Similar results for the DOX-NPs were determined in MCF-7, A549, and HeLa cells.^{38,44} GEN did not show forceful inhibitory effects, as an ancillary drug, towards the RM-1 cells.^{45,46}

APE1 expression at the mRNA level

By evaluating the expression of APE1 at the mRNA level, we found that there was time- and dose-dependent APE1 expression in the RM-1 cells with the treatment of GEN (Fig. S1†). The APE1 levels of the RM-1 cancer cells and 3T3 or L929 normal cells without drug treatment were measured, and the results showed that the RM-1 cancer cells had a higher expression of APE1 than normal cells (Fig. S2†). This suggested that the RM-1 prostate cancer cells had stronger DNA damage repair abilities than normal cells. The intracellular APE1 expression in the RM-1 cells decreased obviously in the GEN, GEN + DOX·HCl, and GEN + DOX-NPs groups as compared to the control group, while there were no statistically significant differences between the GEN, GEN + DOX·HCl, and GEN + DOX-NPs groups (Fig. 3). This suggested that the existence of GEN could reduce the DNA damage repair of the RM-1 cells by downregulating the APE1 expression.

Cellular uptake assessments of DOX-NPs

In Fig. 4, since DOX itself has auto-fluorescent characteristics, the DOX fluorescence signal is detected by FCM in order to investigate cellular uptake without additional fluorescent markers. The fluorescence signal intensity is positively proportional to the amount of DOX internalized by the cells. The

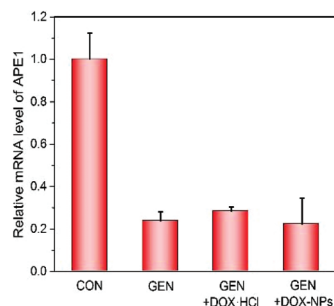


Fig. 3 The relative mRNA level of APE1 in the RM-1 cells with the treatment of drugs ($n = 3$).

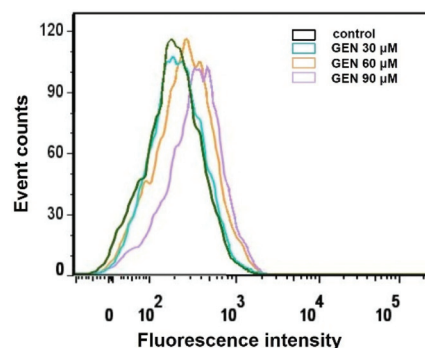


Fig. 5 The intracellular ROS level of the RM-1 cells treated with GEN at pre-defined concentrations.

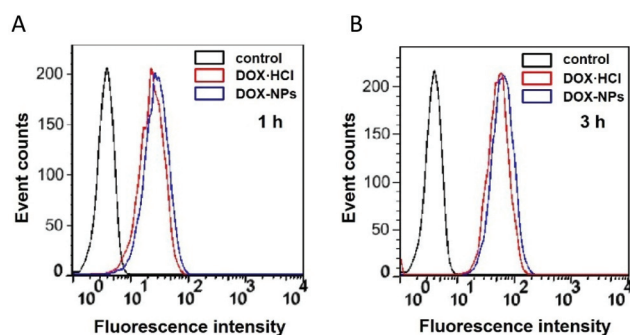


Fig. 4 The cellular uptake of DOX-HCl and DOX-NPs at 1 h (A) and 3 h (B) by FCM.

RM-1 cells were treated with DOX-HCl or DOX-NPs (of equivalent DOX-HCl content). The detected DOX fluorescence signal intensity in the DOX-NPs group was stronger than that of the DOX-HCl group, indicating that the RM-1 cells were inclined towards the cellular uptake of DOX-NPs rather than the free DOX-HCl. The free small molecule doxorubicin hydrochloride was transported into cells *via* passive diffusion, while the DOX-NPs entered into cells mainly by endocytosis.⁴⁷ The FCM analysis results suggested that the uptake of DOX-NPs by the RM-1 cells was more efficient than that of the free DOX-HCl. Both the DOX-HCl and DOX-NPs at 3 h were observed, by analyzing DOX fluorescence signals, to be internalized more than at 1 h, which showed that cellular uptake was a time-dependent behavior.

Cellular ROS level by genistein treatment

The DCFH-DA probe without fluorescence can pass easily through the cell membranes into the cytoplasm and be hydrolyzed into DCFH by intracellular esterase. DCFH is accumulated in the cells and oxidized into fluorescent DCF oxide by intracellular ROS. The green fluorescence intensity detected by FCM is proportional to the ROS level. From Fig. 5, the green fluorescence intensity of the RM-1 cells treated with GEN was dose-dependent – that is to say, the cellular ROS level was gradually improved along with the gradient elevation of GEN. This result can be conjectured to be associated with the influence of APE1. The higher concentration of GEN decreased the

expression of APE1, which reduced the DNA repair and further enhanced the reactive oxygen species.¹⁹

Induction of apoptosis using genistein *in vitro*

As shown in Fig. 6, the apoptosis analysis highlighted that genistein triggered apoptosis depending on the dose of GEN on the whole; the total apoptotic cell proportions were increased along with the increase in GEN concentration. Relatively lower doses were inclined to trigger late apoptosis, while higher doses brought about early apoptosis. At 30 μM GEN, the cell proportions of early apoptosis and late apoptosis were 1% and 3.25%, respectively. The cell proportions of early apoptosis and late apoptosis could be inverted to 11.3% and 2.1% by using a high concentration (120 μM) of GEN. This indicated that the genistein could influence the apoptosis level.

Tumor regression and DOX-NP bio-distribution

To assess the antitumor efficacy *in vivo*, the RM-1 tumor-bearing mice were administered with PBS, GEN, DOX-HCl, DOX-NPs, GEN + DOX-HCl, or GEN + DOX-NPs. In Fig. 7A, it can be seen that the GEN + DOX-NPs group shows an extremely significant inhibition of tumor growth in contrast to the control group. Compared to the other drug treatment groups, the GEN + DOX-NPs group displayed slightly stronger in-

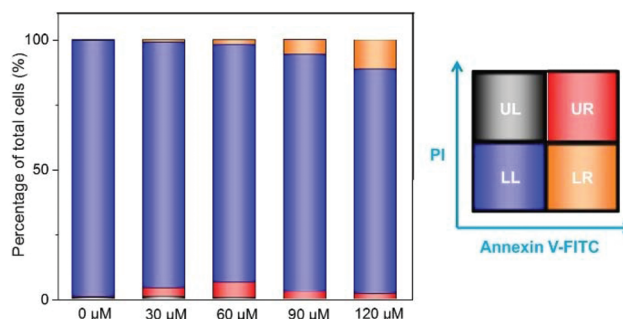


Fig. 6 The cell apoptosis of the RM-1 cells treated with GEN at pre-defined concentrations. The "LR" and "UR" are "lower right" and "upper right" in short, and represent the early cell apoptosis proportion and late cell apoptosis proportion, respectively. The "LL" and "UL" are "lower left" and "upper left" in short, and represent the living cell proportion and cell debris or damaged cell proportion, respectively.

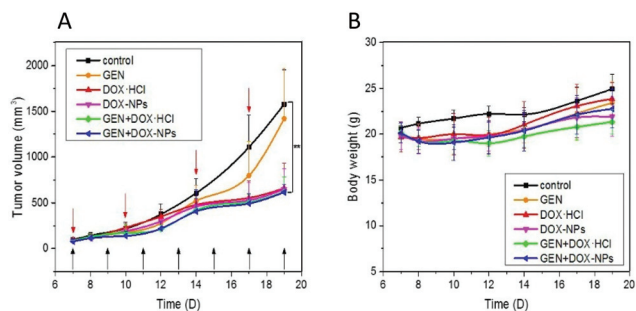


Fig. 7 The anti-tumor evaluation *in vivo* (A) and body weight changes (B). The red arrows represent the application of DOX-HCl or DOX-NPs by *i.v.*, while black arrows represent applications of genistein by *p.o.*

hibition. In order to evaluate the systemic toxicity, the changes in the body weight of the mice are described in Fig. 7B. There were no significant changes in body weight in each group, indicating negligible systemic toxicity against the body weight of mice during the treatment.

The bio-distribution of the free DOX-HCl and DOX-NPs was investigated by examining the *ex vivo* DOX fluorescence images after intravenous administration. As shown in Fig. 8, the DOX fluorescence intensity of the DOX-NPs group at every studied time interval was significantly stronger than that of the free DOX-HCl group at the tumor sites. This phenomenon showed that the DOX-NPs were able to accumulate more at the tumor sites than the free DOX-HCl, resulting in enhanced treatment efficacy. In addition, for the DOX-NPs group, DOX fluorescence in the tumors at 12 h post-injection became slightly stronger compared to that at 2 h and 6 h post-injection, indicating that DOX-NPs exhibited longer blood circulation and less uptake by the reticuloendothelial system, owing to the shielding effect of PEG. At 12 h post-injection, the lower fluorescence signals from the excised heart in the DOX-NPs group could validate a lower cardiotoxicity compared to the DOX-HCl group. For the kidneys, DOX fluorescence signals in the DOX-NPs group had an enhancement at 6 h post-injection and then a fast attenuation at 12 h post-administration, as compared to that of the DOX-HCl group, suggesting that DOX-NPs should have a low influence on the kidneys.

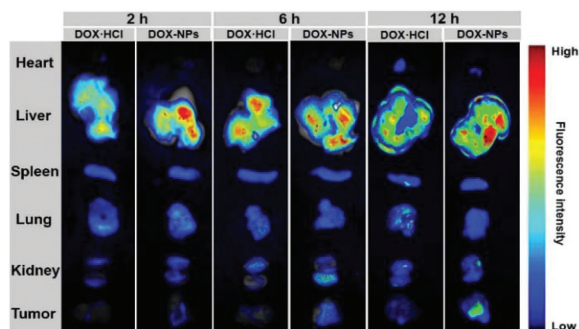


Fig. 8 The tissue distribution of DOX-HCl and DOX-NPs after administration of DOX-HCl and DOX-NPs.

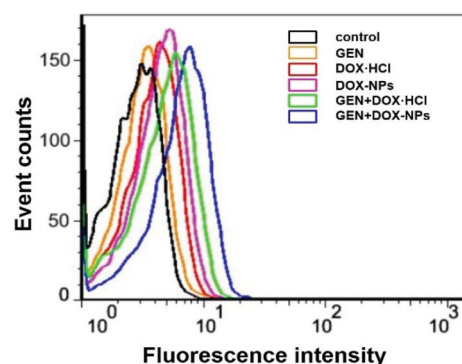


Fig. 9 The ROS level of tumor tissues.

Tumor tissue ROS detection

Emissive green fluorescence intensity was used to evaluate the amount of ROS. As shown in Fig. 9, FCM analysis demonstrated that the RM-1 cells in the GEN + DOX-NPs group were compelled to produce more ROS than those in other groups, as evidenced by the detected strongest green fluorescence signal. The ROS level of the tumor tissue cells at the tumor sites had an obvious increase with the co-administration of GEN and DOX-NPs. The DOX-NPs could induce the production of more ROS than the free DOX-HCl, while GEN could decrease the APE1 level and then amplify the amount of ROS. The co-administration of GEN and DOX-NPs, as a combination blow, could be conjectured to enhance the oxidative damage caused by the high level of ROS.

Histopathological and immune-histochemical analysis in mouse prostate models

As depicted in Fig. 10 and 11, the H&E staining indicated that spontaneous pulmonary metastases occurred in the control

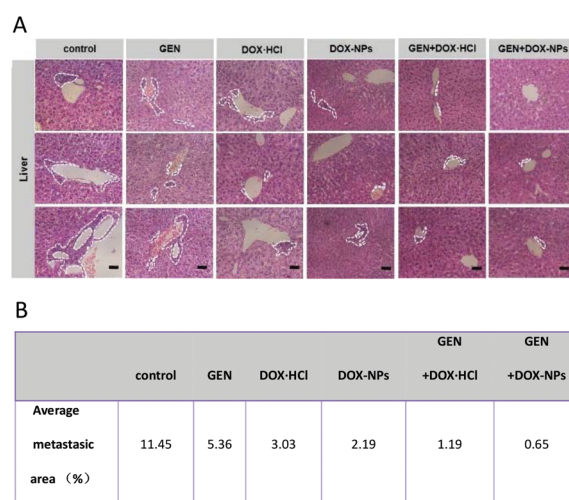


Fig. 10 The pathological analysis of liver metastatic sections (A) and quantification of average metastatic areas (B); scale bars, 100 μm . The dashed white lines in the liver tissues represent metastatic sections.

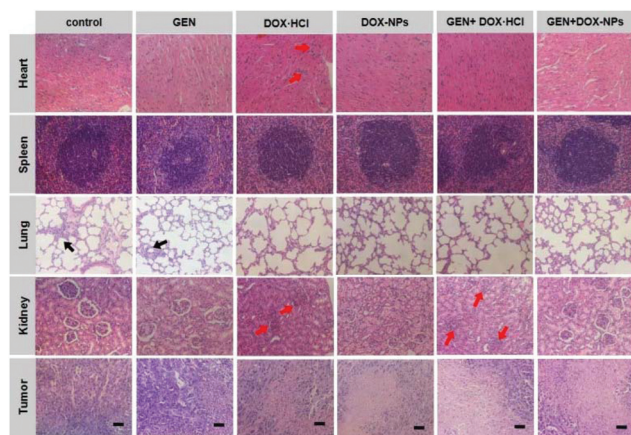


Fig. 11 H&E staining of main organ tissues; scale bars, 100 μm . The black arrows in the lung tissues represent metastatic sections, and the red arrows refer to abnormalities of the tissues.

and GEN groups. The livers had more or less metastatic lesions in all groups. However, these metastatic events could be significantly reduced in the combined groups, including the GEN + DOX-HCl and GEN + DOX-NPs groups; in particular, in the GEN + DOX-NPs group, metastatic areas of the liver tissue showed a remarkable reduction, which could be explained by the notion that tumor cell metastasis was depressed by the enhanced oxidative damage in the combined group.⁹ With regard to the pathological sections in the free DOX-HCl group, abnormal nuclei aggregation and myocardium tissue damage were observed in the heart tissue. However, the DOX-NPs did not trigger these phenomena in the heart, suggesting that DOX-NPs do not have as obvious cardiotoxicity as free DOX-HCl. The partial renal capsule cavity of the kidneys shrank or disappeared in the DOX-HCl and GEN + DOX-HCl groups, but the same phenomena did not occur in the DOX-NPs and GEN + DOX-NPs groups, suggesting that DOX-NPs do not have the same nephrotoxicity as free DOX-HCl. It is worth mentioning that these symptoms could be relieved after the co-administration of GEN and DOX-NPs. As shown in H&E-dyed tumor tissues, the combination of GEN + DOX-NPs could destroy the nuclei integrities and produce more massive necrosis of tumor cells than all the other groups. This further suggested that GEN + DOX-NPs could restrain the growth of tumors.

It is conjectured that the increased ROS could induce the downregulation of APE1.¹⁹ As shown in the immunofluorescence analysis in Fig. 12, the expression of APE1 in the GEN + DOX-NPs group was significantly decreased compared to other groups, suggesting that the combination of GEN and DOX-NPs could reduce damage repair. 8-Oxo-dG was used for labelling the products of DNA oxidative damage by ROS and measuring the oxidative damage levels because the expression of 8-oxo-dG is positively proportional to the oxidative damage level.^{48,49} As shown in Fig. 13, the intracellular 8-oxo-dG level of tumor cells treated with GEN + DOX-NPs was significantly increased, owing to the decrease of APE1 and increase of intracellular

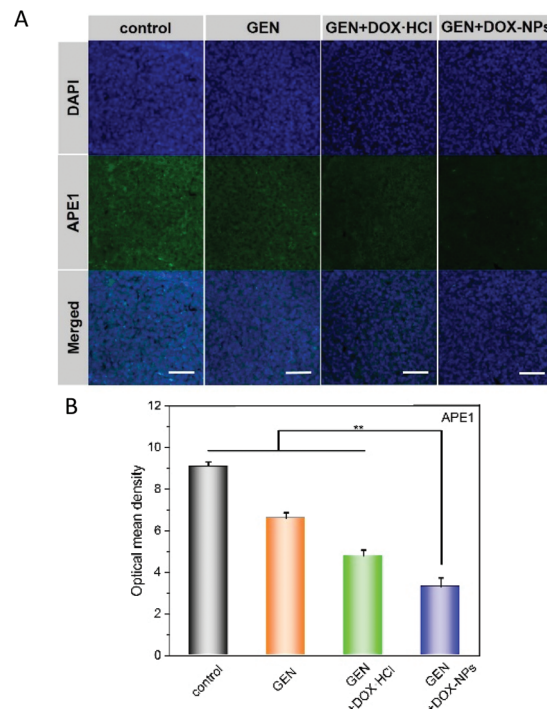


Fig. 12 The APE1 expression of tumor tissues (A) and quantification of the optical mean density (B); scale bars, 100 μm .

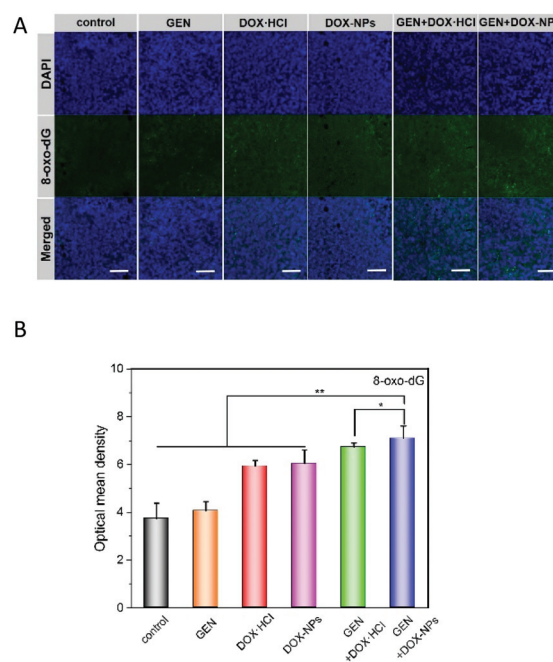


Fig. 13 The 8-oxo-dG level of tumor tissues (A) and quantification of the optical mean density (B); scale bars, 100 μm .

ROS. Enhanced oxidative damage was associated with the combined actions of the decrease of APE1 by GEN and the elevation of ROS by the DOX-NPs. Oxidative damage could

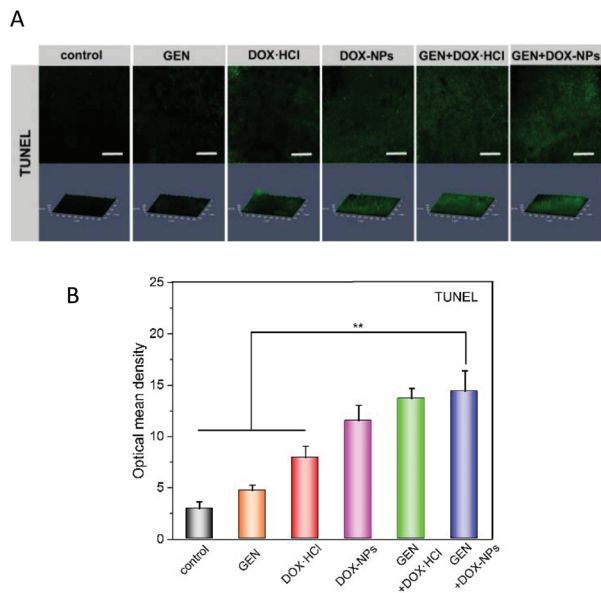


Fig. 14 The assessment of a TUNEL assay at the tumor sites (A) and the quantification of the optical mean density (B); scale bars, 100 μm . The green fluorescence intensity represents the DNA break level.

result in the apoptosis of cancer cells.⁵⁰ Therefore, the co-administration of GEN and DOX-NPs could trigger more apoptosis and produce more DNA breaks that can be detected by a TUNEL assay (Fig. 14).

Conclusions

In this study, a co-administration system of genistein and DOX-NPs was constructed for the treatment of prostate cancer with rapid proliferation and potential metastasis. Based on nanotechnology, the prepared DOX-NPs could improve tumor accumulation and reduce the systemic toxicity compared to free DOX-HCl. Importantly, DOX-NPs could augment the intracellular ROS level in the prostate cancer cells and induce oxidative damage. GEN could assist in the utilization of DOX-NPs by decreasing the expression of APE1 in order to enhance the ROS level and amplify oxidative damage to the prostate cancer cells. Application of DOX-NPs in conjunction with genistein was authenticated as a desired strategy for promoting distinct tumor shrinkage and weakening the metastasis of prostate cancer. Therefore, amplifying oxidative damage is a good choice for the prevention of metastasis in cancer treatment.

Conflicts of interest

The authors declare that there is no conflict of interest.

Acknowledgements

This work was financially supported by the National Natural Science Foundation of China (Projects 51520105004, 51673189, 51390484, 51403204, 51673185, and 51503202), the Science and Technology Service Network Initiative (Project KFJ-SW-STS-166), and the Chinese Academy of Sciences Youth Innovation Promotion Association.

Notes and references

- 1 R. L. Siegel, K. D. Miller and A. Jemal, *CA-Cancer J. Clin.*, 2017, **67**, 7–30.
- 2 G. A. Sonn, W. Aronson and M. S. Litwin, *Prostate Cancer Prostatic Dis.*, 2005, **8**, 304–310.
- 3 A. D. Salaam, P. T. Hwang, A. Poonawalla, H. N. Green, H. W. Jun and D. Dean, *Nanotechnology*, 2014, **25**, 425103.
- 4 K. Zhao, D. Li, W. Xu, J. Ding, W. Jiang, M. Li, C. Wang and X. Chen, *Biomaterials*, 2017, **116**, 82–94.
- 5 H. Zhou, H. Sun, S. Lv, D. Zhang, X. Zhang, Z. Tang and X. Chen, *Acta Biomater.*, 2017, **54**, 227–238.
- 6 H. Sun, J. Su, Q. Meng, Q. Yin, L. Chen, W. Gu, Z. Zhang, H. Yu, P. Zhang, S. Wang and Y. Li, *Adv. Funct. Mater.*, 2017, **27**, 1604300.
- 7 S. Yang, Z. Tang, D. Zhang, M. Deng and X. Chen, *Biomater. Sci.*, 2017, **5**, 2169–2178.
- 8 M. Peiris-Pages, U. E. Martinez-Outschoorn, F. Sotgia and M. P. Lisanti, *Cell Metab.*, 2015, **22**, 956–958.
- 9 E. Piskounova, M. Agathocleous, M. M. Murphy, Z. Hu, S. E. Huddlestun, Z. Zhao, A. M. Leitch, T. M. Johnson, R. J. DeBerardinis and S. J. Morrison, *Nature*, 2015, **527**, 186–191.
- 10 P. T. Schumacker, *Cancer Cell*, 2015, **27**, 156–157.
- 11 X. Li, L. Li, Y. Huang, B. Liu, H. Chi, L. Shi, W. Zhang, G. Li, Y. Niu and X. Zhu, *Biomater. Sci.*, 2017, **5**, 2068–2078.
- 12 I. Matai, A. Sachdev and P. Gopinath, *Biomater. Sci.*, 2015, **3**, 457–468.
- 13 L. C. Mark, R. Kelley, R. Foster, R. Tritt, J. Jiang, J. Broshears and M. Koch, *Clin. Cancer Res.*, 2001, **7**, 824–830.
- 14 D. G. Yoo, Y. J. Song, E. J. Cho, S. K. Lee, J. B. Park, J. H. Yu, S. P. Lim, J. M. Kim and B. H. Jeon, *Lung Cancer*, 2008, **60**, 277–284.
- 15 D. Wang, D. B. Xiang, X. Q. Yang, L. S. Chen, M. X. Li, Z. Y. Zhong and Y. S. Zhang, *Lung Cancer*, 2009, **66**, 298–304.
- 16 J. J. Raffoul, A. R. Heydari and G. G. Hillman, *J. Oncol.*, 2012, **2012**, 370481.
- 17 Y. Seo and T. J. Kinsella, *Cancer Res.*, 2009, **69**, 7285–7293.
- 18 Y. R. S. Preeyaporn Koedrieth, *Mol. Cell. Toxicol.*, 2011, **7**, 389–397.
- 19 S. Jiang, L. Zhu, H. Tang, M. Zhang, Z. Chen, J. Fei, B. Han and G. M. Zou, *Int. J. Oncol.*, 2015, **47**, 610–620.
- 20 S. Sengupta, A. K. Mantha, S. Mitra and K. K. Bhakat, *Oncogene*, 2011, **30**, 482–493.

- 21 M. L. Pinzon-Daza, Y. Cuellar-Saenz, F. Nualart, A. Ondo-Mendez, L. Del Riesgo, F. Castillo-Rivera and R. Garzon, *J. Cell. Biochem.*, 2017, **118**, 1868–1878.
- 22 R. Chattopadhyay, S. Das, A. K. Maiti, I. Boldogh, J. Xie, T. K. Hazra, K. Kohno, S. Mitra and K. K. Bhakat, *Mol. Cell. Biol.*, 2008, **28**, 7066–7080.
- 23 S. Choi, H. K. Joo and B. H. Jeon, *Chonnam Med. J.*, 2016, **52**, 75–80.
- 24 S. S. Laev, N. F. Salakhutdinov and O. I. Lavrik, *Bioorg. Med. Chem.*, 2017, **25**, 2531–2544.
- 25 Y. Jiang, C. Guo, M. L. Fishel, Z. Y. Wang, M. R. Vasko and M. R. Kelley, *DNA Repair*, 2009, **8**, 1273–1282.
- 26 M. L. Fishel and M. R. Kelley, *Mol. Aspects Med.*, 2007, **28**, 375–395.
- 27 M. L. Fishel, Y. He, A. M. Reed, H. Chin-Sinex, G. D. Hutchins, M. S. Mendonca and M. R. Kelley, *DNA Repair*, 2008, **7**, 177–186.
- 28 G. D. Liu, L. Xia, J. W. Zhu, S. Ou, M. X. Li, Y. He, W. Luo, J. Li, Q. Zhou, X. Q. Yang, J. L. Shan, G. Wang, D. Wang and Z. Z. Yang, *Cell Biochem. Biophys.*, 2014, **69**, 725–733.
- 29 A. B. T. Sharon, A. Vantyghem, S. M. Wilson, C. O. Postenka, W. Al-Katib and A. F. Chambers, *Cancer Res.*, 2005, **65**, 3396–3403.
- 30 M. Lakshman, L. Xu, V. Ananthanarayanan, J. Cooper, C. H. Takimoto, I. Helenowski, J. C. Pelling and R. C. Bergan, *Cancer Res.*, 2008, **68**, 2024–2032.
- 31 M. Russo, G. L. Russo, M. Daglia, P. D. Kasi, S. Ravi, S. F. Nabavi and S. M. Nabavi, *Food Chem.*, 2016, **196**, 589–600.
- 32 J. J. Raffoul, S. Banerjee, V. Singh-Gupta, Z. E. Knoll, A. Fite, H. Zhang, J. Abrams, F. H. Sarkar and G. G. Hillman, *Cancer Res.*, 2007, **67**, 2141–2149.
- 33 H. Wu, H. Cabral, K. Toh, P. Mi, Y. C. Chen, Y. Matsumoto, N. Yamada, X. Liu, H. Kinoh, Y. Miura, M. R. Kano, H. Nishihara, N. Nishiyama and K. Kataoka, *J. Controlled Release*, 2014, **189**, 1–10.
- 34 J. M. Horacio Cabral, Yu Matsumoto, P. Mi, H. Wu, T. Nomoto, K. Toh, N. Yamada, Y. Higuchi, S. Konishi, M. R. Kano, R. Hiroshi Nishihara, O. Yutaka Miura, N. Nishiyama and K. Kataoka, *ACS Nano*, 2015, **9**, 4957–4967.
- 35 P. Mi, D. Kokuryo, H. Cabral, H. Wu, Y. Terada, T. Saga, I. Aoki, N. Nishiyama and K. Kataoka, *Nat. Nanotechnol.*, 2016, **11**, 724–730.
- 36 G. Wang, W. Song, N. Shen, H. Yu, M. Deng, Z. Tang, X. Fu and X. Chen, *Sci. China Mater.*, 2017, **60**, 995–1007.
- 37 J.-Y. Zhu, D.-W. Zheng, M.-K. Zhang, W.-Y. Yu, W.-X. Qiu, J.-J. Hu, J. Feng and X.-Z. Zhang, *Nano Lett.*, 2016, **16**, 5895–5901.
- 38 S. Lv, M. Li, Z. Tang, W. Song, H. Sun, H. Liu and X. Chen, *Acta Biomater.*, 2013, **9**, 9330–9342.
- 39 D. Shao, M. Lu, D. Xu, X. Zheng, Y. Pan, Y. Song, J. Xu, M. Li, M. Zhang, J. Li, G. Chi, L. Chen and B. Yang, *Biomater. Sci.*, 2017, **5**, 1820–1827.
- 40 S. Lv, Z. Tang, M. Li, J. Lin, W. Song, H. Liu, Y. Huang, Y. Zhang and X. Chen, *Biomaterials*, 2014, **35**, 6118–6129.
- 41 W. Song, Z. Tang, D. Zhang, X. Wen, S. Lv, Z. Liu, M. Deng and X. Chen, *Theranostics*, 2016, **6**, 1023–1030.
- 42 H. Cabral, Y. Matsumoto, K. Mizuno, Q. Chen, M. Murakami, M. Kimura, Y. Terada, M. R. Kano, K. Miyazono, M. Uesaka, N. Nishiyama and K. Kataoka, *Nat. Nanotechnol.*, 2011, **6**, 815–823.
- 43 J. Chen, J. Ding, C. Xiao, X. Zhuang and X. Chen, *Biomater. Sci.*, 2015, **3**, 988–1001.
- 44 N. Shen, J. Jiang, D. Zhang, G. Wang, S. Lv, Y. Jia, Z. Tang and X. Chen, *ACS Biomater. Sci. Eng.*, 2017, DOI: 10.1021/acsbomaterials.7b00639.
- 45 Y. Yang, A. Zang, Y. Jia, Y. Shang, Z. Zhang, K. Ge, J. Zhang, W. Fan and B. Wang, *Oncol. Lett.*, 2016, **12**, 2189–2193.
- 46 T. Roh, S. W. Kim, S. H. Moon and M. J. Nam, *Food Chem. Toxicol.*, 2016, **97**, 127–134.
- 47 M. Prabakaran, J. J. Grailer, S. Pilla, D. A. Steeber and S. Gong, *Biomaterials*, 2009, **30**, 5757–5766.
- 48 J. Sheridan, L. M. Wang, M. Tosetto, K. Sheahan, J. Hyland, D. Fennelly, D. O'Donoghue, H. Mulcahy and J. O'Sullivan, *Br. J. Cancer*, 2009, **100**, 381–388.
- 49 C. C. Sung, Y. C. Hsu, C. C. Chen, Y. F. Lin and C. C. Wu, *Oxid. Med. Cell. Longevity*, 2013, **2013**, 301982.
- 50 H. B. Ruttala, N. Chitrapriya, K. Kaliraj, T. Ramasamy, W. H. Shin, J. H. Jeong, J. R. Kim, S. K. Ku, H. G. Choi, C. S. Yong and J. O. Kim, *Acta Biomater.*, 2017, **63**, 135–149.